

ANGULAR RESOLUTION STUDY
OF THE ATLAS LAR CALORIMETER
FOR NON-PROJECTIVE PHOTONS
WITH 2004 TEST BEAM DATA

—

A STUDY ON THE DISCOVERY POTENTIAL OF ATLAS
FOR THE $\tilde{\chi}_1^0 \rightarrow \gamma\tilde{G}$ DECAY IN GMSB SUSY MODELS*

CERN SUMMER STUDENT PROJECT 2005

performed by:

O. Brandt

University of Bonn, oleg.brandt@cern.ch

supervisors:

Imma Riu Dachs

University of Geneva, imma.riu@cern.ch

Oliver Gaumer

University of Geneva, olivier.gaumer@cern.ch

October 24, 2005

Abstract

After a brief introduction to ATLAS physics with an emphasis on GMSB SUSY models and in particular on the $\tilde{\chi}_1^0 \rightarrow \gamma\tilde{G}$ decay channel, the ansatz for its detection using the photon only will be introduced.

In the second part of the report the angular resolution of the EM calorimeter of ATLAS for ~ 60 GeV photons, as expected for the $\tilde{\chi}_1^0 \rightarrow \gamma\tilde{G}$ decay, will be focused, which is crucial for the discovery potential for GMSB SUSY.

A new method for determining the non-projectivity of the photon and thus its impact angle utilizing only one sampling will be introduced and tested for its performance. The same will be done for the conventional two-sampling method. Next, both methods will be evaluated.

*also available at <http://www.nikhef.nl/~x50/cern/NonPointingPhotonsResolution.2005Project.pdf>

At the end, a rough estimate for the discovery potential of GMSB SUSY at ATLAS will be given.

1 Physics at ATLAS

ATLAS is one of the two main experiments in preparation at CERN. It will analyse collision data of the Large Hadron Collider, an enormous proton-proton accelerator with absolutely remarkable benchmarks: a design luminosity of $10^{34} \text{ cm}^{-2}\text{s}^{-1}$ and a center of mass collision energy of 14 TeV [6]. Regarding the parton distribution functions, this machine will grant us access to an energy scale of several hundreds of GeV's, which should allow the long awaited discovery of the Higgs boson, as according to LEP $m_{\text{Higgs}} > 113.5 \text{ GeV}$ at 2σ confidence level. Though, the LHC will focus even more extremely interesting phenomena: for example some subset

of Super SYmmetric (SUSY) models, with the discovery potential for the Gauge Mediated Symmetry Breaking (GMSB) model decay $\tilde{\chi}_1^0 \rightarrow \gamma\tilde{G}$ being the subject of this report. SUSY theories are under discussion as an extension to the Standard Model (SM) of Particle Physics, reducing the number of free parameters to as few as 6. Their main feature are supersymmetric partners to each particle of the SM sector, where the partners of fermions are bosons and vice versa. The masses of lightest SUSY particles are of $\mathcal{O}(300\text{ GeV})$. A subclass of SUSY models are the GMSB models.

The ATLAS detector itself is outstanding as well: it is a multi-purpose detector with 4π solid angle coverage, low noise level electronics and a high resolution for energy and position [1]. In order to achieve high resolution and linearity combined with reasonable costs and radiation hardness, the ElectroMagnetic (EM) calorimeter is an ionisation chamber with liquid argon acting as an active substance, accordion-shaped copper electrodes on capton and lead plates as conversion material [2]. It consists of 3+1 samplings with different granularity and depth: s1 being the strips, s2 the middle and s3 the back, plus a presampler indexed as s0, which should recover upstream energy losses in dead material.

1.1 The $\tilde{\chi}_1^0 \rightarrow \gamma\tilde{G}$ Decay Channel in GMSB SUSY Models and Its Detection

Now, as already mentioned, the angular resolution study in focus of this report is mainly important in order to investigate the discovery potential of the ATLAS detector for the $\tilde{\chi}_1^0 \rightarrow \gamma\tilde{G}$ reaction in GMSB SUSY models, which should be observable at $Q_{\text{LHC}} \cong \mathcal{O}(300\text{ GeV})$ for a specific set of the six free parameters. Let us briefly review some basic facts about GMSB models: the symmetry breaking occurs at a high energy scale $\sqrt{F_0}$ and is translated via chiral superfields to the so-called messenger sector, which again transfers the symmetry breaking to the well-understood SM sector via $\text{SU}_C(3) \otimes \text{SU}_L(2) \otimes \text{SU}_Y(1)$ gauge bosons (thus the name GaugeMediatedSB). One of the 6 parameters of the theory is the messenger sector energy scale $\sqrt{F_0}$.

In our scenario the gravitino \tilde{G} is the lightest SUSY particle (LSP), so all the other particles of the supersymmetric sector will decay to it, in particular the neutralino $\tilde{\chi}_1^0$, being the next-to-LSP (NLSP). As \tilde{G} interacts only gravitationally, the ATLAS detector will not see it. Thus, we will be able to detect the photon only, which gives us a signature for this reaction: missing energy $E_{\text{miss}} \cong m_{\tilde{G}} \cong \mathcal{O}(300\text{ GeV})$. Now, what kind of photon are we looking for? Its energy should be

of the order of the mass difference between the neutralino and the gravitino: $E_\gamma \cong m_{\tilde{\chi}_1^0} - m_{\tilde{G}} \cong 50\text{ GeV}$.

A very special feature to the GMSB models is, that for a specific set of free parameters, the decay length of the neutralino can be macroscopic: $c\tau_{\tilde{\chi}_1^0} \in [1\mu\text{m} \dots 100\text{ m}]$. Thus we should look out for so-called *non-projective*¹ photons which originate a certain distance away from the DIP. An example of the complete decay chain can be seen in fig. 1. A non-projective photon is a good signature as well (the higgs for example gives two high energetic photons, but its decay length is very small). In terms of precision and experimental accessibility it is convenient to restrict the analysis to a scenario where the produced neutralino travels along the z-axis (the direction of the beamline) or with a small deviation from it. What is most interesting about the mean path length of the neutralino, is its connection to other GMSB SUSY parameters via:

$$c\tau_{\tilde{\chi}_1^0} = \frac{1}{k_\gamma} \left(\frac{100\text{ GeV}}{m_{\tilde{\chi}_1^0}} \right)^5 \left(\frac{\sqrt{F_0}}{100\text{ TeV}} \right)^4 \cdot 10^{-2}\text{ cm},$$

where $k_\gamma := |N_{11} \cos \theta_W - N_{12} \sin \theta_W|$, θ_W is the Weinberg angle and N_{ij} the mixing angles of the neutralinos [4].

We can access $c\tau_{\tilde{\chi}_1^0}$ using the data of the photon only by the combination of the angle of non-projectivity (α in fig. 1) with the time difference between the $p\bar{p}$ interaction and the signal in the EM calorimeter. To determine the angle of non-projectivity α one can use the data of the EM calorimeter only, as non-converted photons cannot be seen in the tracker. Clearly, a good understanding of the error to the angle measurement with the EM calorimeter is the essential keypoint. Its analysis using the 2004 Combined Testbeam data is the subject of this report. At the end it will be compared with detailed ATLAS MC simulation results presented in [4].

1.2 ATLAS 2004 Test Beam Setup

Before we present the analysis methods applied and their results, a short overview of the ATLAS 2004 Test Beam Setup shall be given. It was the first test beam run, in which segments of all future components of ATLAS have been installed and could be tested simultaneously with beams of several particles.

In the runs used for this analysis a positron beam with $E_{\text{beam}} = 180\text{ GeV}$ was shot onto a

¹the term "non-projective" refers to the fact, that the cells of the EM calorimeter point or *are projecting* towards the Designed Interaction Point (DIP) in order to minimize the number of cells fired to improve the statistics and thus the resolution

thin conversion foil in order to produce photons via bremsstrahlung processes in the coulomb field of the lattice. From this point positrons and photons travel for almost 20 m on the same trajectory to the separation magnets, where positrons are bent away with respect to photons. Please refer to the sketch of the setup in fig. 2; and for more details, in particular on the additional beamline instrumentation, to [3]. After having travelled approximately 8 meters and having traversed the inner detector (with its magnet being off) the particles hit the EM calorimeter at two different spots. As the positrons and photons are separated at a point which is roughly 8 meters away and not in the DIP of ATLAS (distance: roughly 1.5 m), a slightly different non-projectivity is expected for them. Clearly, one can position the calorimeter in a projective way for only one type of particles, in our comparison run (#2102966) it were the photons.

How was non-projectivity studied with this setup? The calorimeter was tilted in such a way, that it would be projective for photons hitting it at a position of $\eta_{\text{tilt}} = 0.3$, $\hat{\theta}(\eta)^2 = 73.1^\circ$, $\theta := 90^\circ - \hat{\theta} = 16.9^\circ$, and moved perpendicular to the test beam line in steps of $\Delta d = 20$ cm, which results in a slightly larger distance of non-projectivity $d_z = d/\cos(\theta)$ with respect to the DIP³, as $\Delta d_z = \Delta d/\cos(\theta) = 20.91$ cm. The key data for non-projective runs analyzed in the framework of this project and a comparison run are summarized in tab. 1.

2 Photon Spectrum Selection

Before we can come to speak about the analysis methods and their results in the next chapter, let me describe briefly how a proper photon spectrum, suitable to study the angular resolution of the ATLAS detector, was selected. Clearly, the most optimal choice would be a Dirac distribution centered around an expected photon energy of roughly 60 GeV. To obtain something which comes closest to this optimum situation, a copper foil was chosen with its mean coulomb field of the lattice having exactly the right strength to give a photon spectrum consisting of two parts: a gaussian-like distribution centered around somewhat more than 60 GeV with a FWHM of roughly 10 GeV, and another part

² $\hat{\theta}$ is defined according to canonical polar coordinates conventions in the coordinate system of the TestBeam (TB), with the z_{TB} -axis being orientated along the beamline

³here z is the axis defined by the beamline of ATLAS, with the EM calorimeter in its future position, thus it is parallel to the surface of the EM module and is oriented towards rising η

dropping towards lower energies, which will be cut away later. In the whole analysis the topo clustering algorithm with the default seed set of $(4\sigma, 2\sigma, 0\sigma)$ and the "all3D" option was used, and version 10.0.4 of ATLAS software. For all runs an initial dataset of 25000 events was taken.

Several ways to cut on events with radiated photons were investigated, and the performance of the algorithm described below found to be best. Basically, the procedure to select the events consists of two parts: first, the positions of energy-weighted⁴ η -positions of all "good" clusters was plotted in a η - φ scatterplot. Since for these events the kinematics is fixed, we obtain a strong accumulation of histogram entries around a certain η - φ value for the electrons and the same for photons. In the second step one cuts *geometrically* on the η -positions of the clusters. Since the geometrical cuts are quite tight and the kinematics of photon production events is *very* special, as there are no particles in the mass range of the electrons, we remove very efficiently also the background of pions and MIP's, as you can see from fig. 5 for run #'89.

Now, what is a "good" cluster? The definition of a "good" cluster follows from kinematics: since we expect the photon to have an energy of around $\langle E_\gamma \rangle = 60$ GeV and accordingly for the electron $\langle E_{e^+} \rangle = 180 \text{ GeV} - 60 \text{ GeV} = 120$ GeV, we require the electron cluster to have an energy (introducing a spread of ± 15 GeV) between 105 and 135 GeV:

$$105 \text{ GeV} \stackrel{!}{<} E_{\text{cluster}}^{e^+} \stackrel{!}{<} 135 \text{ GeV},$$

whereas the photon cluster should have more than 30 GeV:

$$E_{\text{cluster}}^\gamma \stackrel{!}{>} 30 \text{ GeV}.$$

In the previous lines, I have been speaking about an electron and a photon cluster, how can we a priori distinguish them? The answer is fast forward – the topo clustering algorithm sorts the clusters according to their energies, thus in events we are looking for, i.e. where a photon conversion has occurred, the electron will always have more energy and thus be the first cluster.

Having done this, we obtain, as already mentioned, an η - φ scatterplot which looks similar to the one shown in fig. 3 for run #'89. You can see a strong accumulation around certain η - φ values for both the electron and the photon cluster. All one has to do now is to impose some geometrical cuts, which do a good compromise between removing efficiently the undesired background and leaving as many events as possible. All the cuts for analyzed runs can have been summarized in

⁴for definition of $\langle \eta \rangle_{\text{energy}}^j$ see subparagraph 3.1

table 2. After applying the cuts to the dataset we obtain spectra, which are shown in fig. 4. Except for run #'86, they all look quite good, and with some minor deviations we see what we expected from the description at the beginning of this section.

Though, we also see a clear difference between the photon spectrum of run #'86 and other runs: on the one hand, the peak of the spectrum is shifted towards lower energies by some 5-10 GeV, on the other hand the distribution is much wider (percentually, scaled with the peak height). The reason can be seen on fig. 6: unfortunately, for "good" events the photons hit exactly two dead cells of the calorimeter in sampling 1, which registers approx. 20-30 GeV of the total EM energy or some 5-10 GeV of the energy of the photon. Like this, a major fraction of the photon energy, which is contained in the middle of the shower is not seen at all, which account for the missing 10 GeV in the photon spectrum and in the total energy as well. As we are interested photons and sampling 1 is essential for their analysis, run #'86 will not be considered in the following analysis.

To see how good the geometrical selection algorithm performs and how many potentially good events we cut away, the number of "good" electron and photon clusters has been printed before and after the application of the cuts. Their ratio is approx. 5:4 for both the electrons and photons (they were looked at separately), which is a good value regarding the spread width of cluster barycenters in the η - φ scatterplot and a contamination with hadronic events before the cut (clearly, e.g. a pion can give a cluster of 120 GeV after a hadronic interaction). This confirms the event cleaning method once again.

Finally, the lower part of the resulting photon spectrum is cut away at an energy of $E_\gamma \stackrel{!}{>} 55$ GeV. At the end we obtain approximately a gaussian distribution with a FWHM of 10 GeV for both the photons and electrons, as their total energy should not be significantly more than 180 GeV of the beam. The whole procedure reduces our sample to about 15-20% of the initial size.

There are two last cuts of minor importance to be mentioned. One of them requires the number of clusters to be 2 or more than 2⁵, which is due to a bug in Athena software. Let me explain it with an example: if there are two consecutive events in a run, the first run has 2 clusters and the second run only 1, for the second run the variable for the photon cluster energy, i.e. the energy of the second cluster will be filled with the value from

⁵it happens quite often that one has some additional clusters with energies lower than 0.5 GeV. A cut on them was studied but found not to have any significant impact on the photon spectra, except for lowering the statistics

the first run, even though only one cluster was found. In other words, it is a back door for one-cluster events to pass the cut. The other minor cut is the requirement for the energy to be more than 150 GeV.

3 Analysis Methods and Results

Now, as we have selected a proper photon spectrum, we can proceed to the actual measurement of the angular resolution of the ATLAS EM calorimeter. There are two methods, which take different approaches. One of them is quite intuitive: it uses the information of two samplings and combines the η positions of a cluster in both of them. The other method uses the information of a single sampling only and utilizes the information one can extract from the transversal shower shape. In the following, I will refer to these two methods by *two* or *single sampling method*.

3.1 Single Sampling Analysis Method for Non-Projective Photons

As already mentioned, in the single sampling method one uses the fact, that the longitudinal profile of an EM shower can be described by an ellipse, with most of the energy deposited along the initial trajectory of the particle, as indicated on fig. 11.

Now, what happens if a non-projective charged particle *enters*⁶ the EM calorimeter? First, we have to consider, that the beginning of the shower can be approximated by a cone centered around the initial trajectory, which, because of the non-projectivity, is tilted with respect to the inner cell structure of the calorimeter (see fig. 7 to visualize the situation). This results in an asymmetric energy deposit in the calorimeter cells with respect to the energy weighted barycenter of the cluster, which in the first approximation will be proportional to non-projectivity. A good measure to quantify the asymmetry A was found to be⁷

$$\begin{aligned} A &:= \langle \eta \rangle_{\text{energy}}^j - \langle \eta \rangle_{\text{geom}}^j \\ \langle \eta \rangle_{\text{energy}}^j &:= \frac{\sum_i E_i \eta_i}{\sum_i E_i}, \\ \langle \eta \rangle_{\text{geom}}^j &:= \frac{1}{N} \sum_i \eta_i, \end{aligned}$$

where i indexes all cells of a particular cluster in sampling j . Regarding this index set, please keep

⁶this situation applies to the presampler, the strips and the very beginning of the middle sampling

⁷another possibility, which shows a similarly good performance, is to take the η -position of the cell with maximum energy deposit instead of $\langle \eta \rangle_{\text{energy}}^j$

in mind, that a topological clustering algorithm has been used and thus the transversal shower shape in a particular cluster varies from event to event. Thus the asymmetry A gives the displacement of the barycenter with respect to the cluster profile. To illustrate the situation a cluster in the presampler for a particular event in run #2102984 is shown in fig. 7; the color represents the energy deposit. This run corresponds to a negative non-projectivity, i.e. the calorimeter is displaced with respect to the beam by -20.9 cm. As we expected, the barycenter is displaced to the left too, since the incidence direction is tilted to the left with respect to the inner structure of the calorimeter.

Let us take a look at the resulting plots of the asymmetry A for analyzed runs (#'84/-20.9 cm: fig. 8; #'85/+20.9 cm: fig. 9; #'89/+41.8 cm: fig. 10), where the first 3 samplings⁸ (s0-s2) were considered. In each of the plots we have in red the A -distribution of the comparison run #'66, in blue of the analyzed run.

In the following electrons and photons in each of the samplings using the example of run #'89 will be compared. In the presampler (s0) we see a clear separation of the two electron distributions. It is not the case for photons, the #'89 distribution is slightly broader and less regular. We can understand this by the fact, that electrons start to deposit ionization as soon as they enter the calorimeter, whereas for photons the start of the shower is rather a statistical process in the longitudinal direction. The slight asymmetry of the electrons for run #'66 is due to a small non-projectivity, as explained in subparagraph 1.2. The strips (s1) show a much more homogeneous picture: as expected, the difference between electrons and photons vanishes; further, there is a clear separation between the two runs for both particles. A small bump to the left of the main peak in the #'89 photon plot can be traced back to be caused by a hardware problem, since it appears in the strips only, and we have a similar picture for the middle sampling of run #'84. Now, if we take a look at the middle (s2), we see the two blue distributions moving back towards the red distribution again. How can we understand this? The middle sampling has a length of $\mathcal{O}(10X_0)$, thus with a high probability the end of the shower will be contained in it. Since its longitudinal shape is ellipse-like, we can argue in a "reversed" way with respect to the argumentation at the beginning of this subparagraph, which gives us an effect opposite to the one our analysis bases on. Though, the situation in s2 can be improved by introducing a cut on cells containing less than ca. 50 MeV of energy (the noise level is

25 MeV); how exactly this effect can be explained has to be investigated a way further. Summing up, we conclude, that the asymmetry of sampling 1, the strips, is the most suitable measure of non-projectivity for photons. A point for further investigation might be a check for correlations between the samplings for the same event, as then one might combine the data of several samplings to gain a larger statistical basis.

Finally, let us evaluate this method. First, the asymmetry of the three runs for photons in s1 shall be compared. We see a clear dependance of the mean $\langle A \rangle$ on the non-projectivity. The dependance of the two variables seems to be linear, but for a definitive statement runs with larger non-projectivities are needed. The same would be needed to set up a function relating the angle of non-projectivity to A . The error of this method is quite large, but it decreases with rising non-projectivity: the distribution move apart, whereas their widths stay the same.

3.2 Two Sampling Analysis Method for Non-Projective Photons

The basic idea behind the two sampling method is shown in fig. 11: one uses the energy weighted barycenter of the shower for two different samplings, which we expect to give two different coordinates in eta due to non-projectivity. But how can we extract the vector of incidence from it? Clearly, we need one more coordinate in the longitudinal direction of the shower for each of the samplings in order to obtain two 3-dimensional vectors to define the vector of incidence. As we work with the energy weighted mean in the transversal direction, it makes sense to use an energy-weighted mean measured from the future beamline of ATLAS in the longitudinal direction for each of the samplings as well: the shower depth R_i for the i -th sampling. A geometrical analysis of fig. 11 yields a relationship for the angle of incidence θ' , as defined above:

$$\begin{aligned} \tan \theta' &= \frac{R_2 - R_1}{z_2 - z_1} \\ z_i &:= R_i \sinh \eta_i \end{aligned}$$

The shower depth parametrization is a function of the η -position (follows from geometrical arguments) and the energy: $R_i = R_i(\eta, E)$. For this analysis a shower depth parametrization produced with a full GEANT simulation for 50 GeV photons was used⁹. Further, only two coordinates of two samplings, the strips and the middle, were

⁸s3 was not considered, as the shower profile loses its information content due to fluctuations on the way there

⁹in the implementation of the second sampling method with a kind permission of D. Prieur a part of his analysis program implemented. For details, see [4]

analyzed, as the presampler and the back sampling have a quite coarse granularity in η .

Let us come to the results of the two sampling method. For each run the reconstructed angle of incidence θ' was plotted in degrees and fitted with a gaussian, its σ parameter is considered to be the statistical error of the photon incidence angle reconstruction. The histograms for the reconstructed angle can be found in fig. 13. The results meet our expectation – we obtain a symmetric distribution, its shape is very well described by a gaussian. Though, we also see a major problem. The reconstructed angle is not the one we expect, as $\theta' \stackrel{!}{=} 16.9^\circ$. There are two systematic errors which account for this. On the one hand, the shower depth parametrization used was $R_i = R_i(\eta, E \equiv 50 \text{ GeV})$, whereas $\langle E_\gamma \rangle \cong 62 \text{ GeV}$; so R_i is too small. On the other hand, the proper use of this method requires a detailed knowledge of the gain of each particular cell, dead cells etc., since a hot or a high-gain cell can shift the barycenter systematically. Both errors can be minimized easily with a more detailed analysis.

If we compare the resolution plots with each other, we realize that the statistical error for the reconstructed angle rises with larger non-projectivity. This can be explained by the fact, that for a larger non-projectivity the energy deposit will be distributed over a larger number of cells, which worsens the statistics, as the signal has a Poisson distribution for each of the cells. The angular resolution for photons has been summarized in fig. 12, where it is compared¹⁰ with the analysis results found in [4]. We see that the resolution curve presented in this report stays in the same range as the MC prediction and that the general trend is reproduced well – the resolution worsens with rising non-projectivity. Due to missing correction implementation the angular resolution for projective particles, being $50\text{-}60 \text{ mrad}/\sqrt{E[\text{GeV}]}$, cannot be reached. Summarum we can say that in the sense of the footnote below the MC prediction could be confirmed with the 2004 Combined Test Beam data.

4 Summary & Conclusions

In the framework of the CERN 2005 Summer Student Project presented in the underlying report a new measure for non-projectivity of photons has been developed: the single sampling method. Its performance and the performance

¹⁰the word "comparison" should not be taken too seriously here, as my analysis was done without any corrections, e.g. the S-shape, and even a different clustering algorithm – EM.TB – has been used by D. Prieur. The plot is rather intended to give a rough indication for the result evaluation

of the two-sampling method have been studied with ATLAS 2004 Combined Testbeam data. It has been found that the two-sampling method performs significantly better. Though, its error rises with non-projectivity, whereas the opposite is true for the single sampling method. Thus, for large non-projectivity of 1 m and more it makes sense to combine the two methods. Further, an angular resolution of $\mathcal{O}(1.5^\circ)$ degrees for 60 GeV photons and small non-projectivities has been found for the two-sampling method: fig. 12. We conclude, that ATLAS will be able to confirm some GSMB SUSY models with mean path length of the neutralino of roughly between few centimeters and several meters.

References

- [1] *ATLAS Coll.*: ATLAS Detector and Physics Performance Technical Design Report CERN/LHCC/99-14
- [2] *ATLAS LARG Unit*: Liquid Argon Calorimeter Technical Design Report CERN/LHCC/96-41
- [3] *B. di Girolamo et al.*: Beamline Instrumentation in the 2004 Combined ATLAS Testbeam internal note
- [4] *D. Prieur*: Calibration of the ATLAS electromagnetic calorimeter. Reconstruction of events with non pointing photons in SUSY GSMB models. LAPP-T-2005-03
- [5] *J. Colas et al.*: Position Resolution and Particle ID with the ATLAS EM Calorimeter. arXiv:physics/0505127 v1 12 May 2005
- [6] *S. Eidelman et al.*: Review of Particle Physics online (<http://pdg.lbl.gov/>) CERN and LBNL (2004)

Acknowledgements

I would like to thank literally everyone from the ATLAS Combined Test Beam group, as everyone has helped me with this report in this or the other way. I am very grateful for fruitful discussions with Isabelle Wingerter, Karina Laureiro, Martin Aleksa, Martin Pohl and also with Damien Prieur from LAPP. Of course, I would like to thank most my primary supervisor, Imma Riu Dachs and my "unofficial" supervisor Olivier Gaumer for the many discussions, hints and their strong support.

Appendix A: Tables

Run number	η_{tilt}	d_z [cm]	remarks
2102983	0.3	-20.91	
2102984	0.3	-20.91	same setup as for '83
2102985	0.3	+20.91	
2102986	0.3	+41.81	
2102989	0.3	+62.72	was not analyzed, as the photons hit exactly two dead cells
2102966	0.45	0	comparison run, same settings for the separation magnets

Table 1: List of runs analyzed in the framework of this Summer Student Project. For all runs the magnet inside of the inner detector was off, the settings for the separation magnets were: MBPL H: -500 A, MBPL V: 500 A

Run number	$\eta_{\text{min}}^{e^+}$	$\eta_{\text{max}}^{e^+}$	$\varphi_{\text{min}}^{e^+}$	$\varphi_{\text{min}}^{e^+}$	$\eta_{\text{min}}^{\gamma}$	$\eta_{\text{max}}^{\gamma}$	$\varphi_{\text{min}}^{\gamma}$	$\varphi_{\text{min}}^{\gamma}$
2102983	0.085	0.110	0.050	0.070	0.165	0.190	-0.005	0.020
2102984	0.085	0.115	0.050	0.070	0.160	0.195	-0.005	0.020
2102985	0.315	0.340	0.050	0.070	0.395	0.042	-0.010	0.020
2102986	0.535	0.565	0.045	0.070	0.610	0.635	-0.005	0.015
2102989	0.430	0.450	0.050	0.070	0.505	0.535	-0.010	0.020
2102966	0.310	0.340	0.050	0.070	0.390	0.420	-0.010	0.020

Table 2: Geometrical cuts for mean energy weighted positions of the clusters $\langle\eta\rangle_{\text{Energy}}$, $\langle\varphi\rangle_{\text{Energy}}$ in the middle sampling (s2) applied

Appendix B: Figures

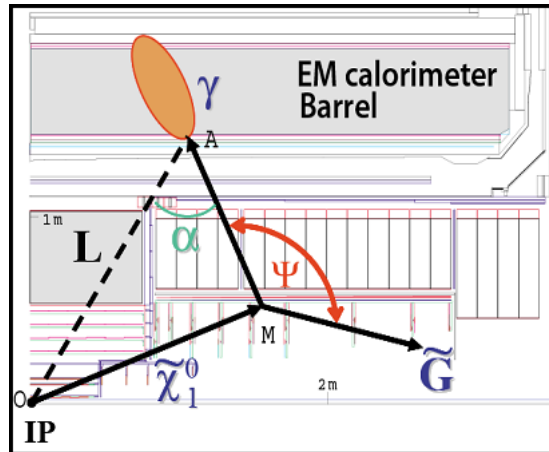


Figure 1: Example scenario for the neutralino decay in GMSB SUSY models.

The angle of emission of the photon has a broad distribution and the kinematic situation shown is realistic, as the two supersymmetric particles have similar masses; i.e. the masses are much larger than their difference, that is the photon energy. The analysis is restricted to events only, in which the neutralino travels in a small cone around the axis, as in the contrary case the chance for the photon to convert in the tracker is much larger and thus one cannot be sure that *it is* a photon at all.

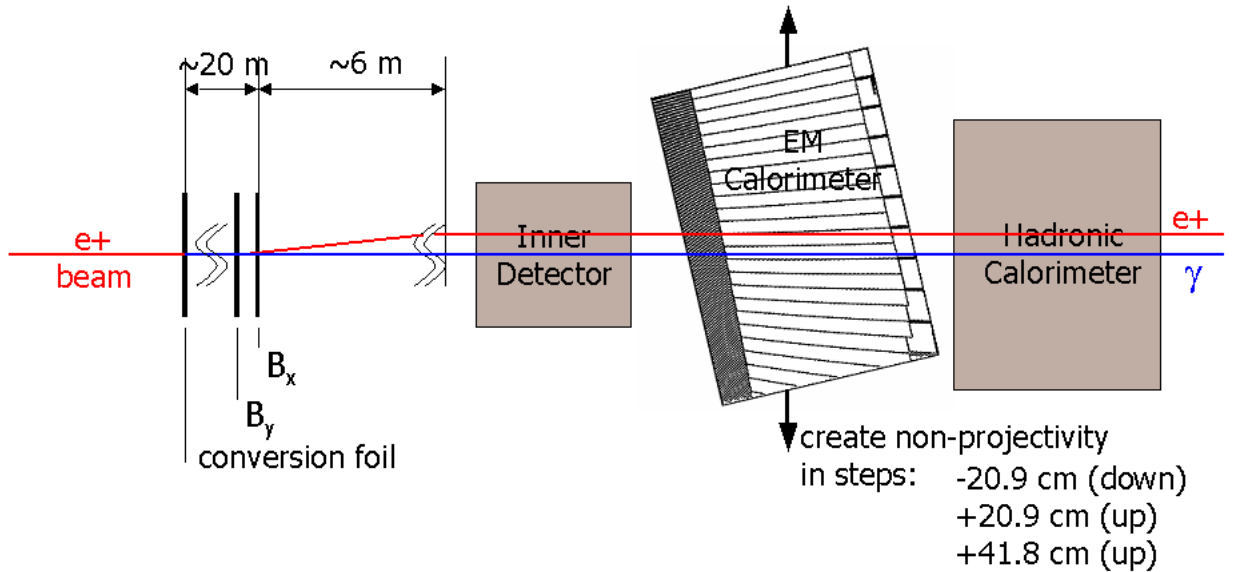


Figure 2: ATLAS 2004 Combined Test Beam setup.

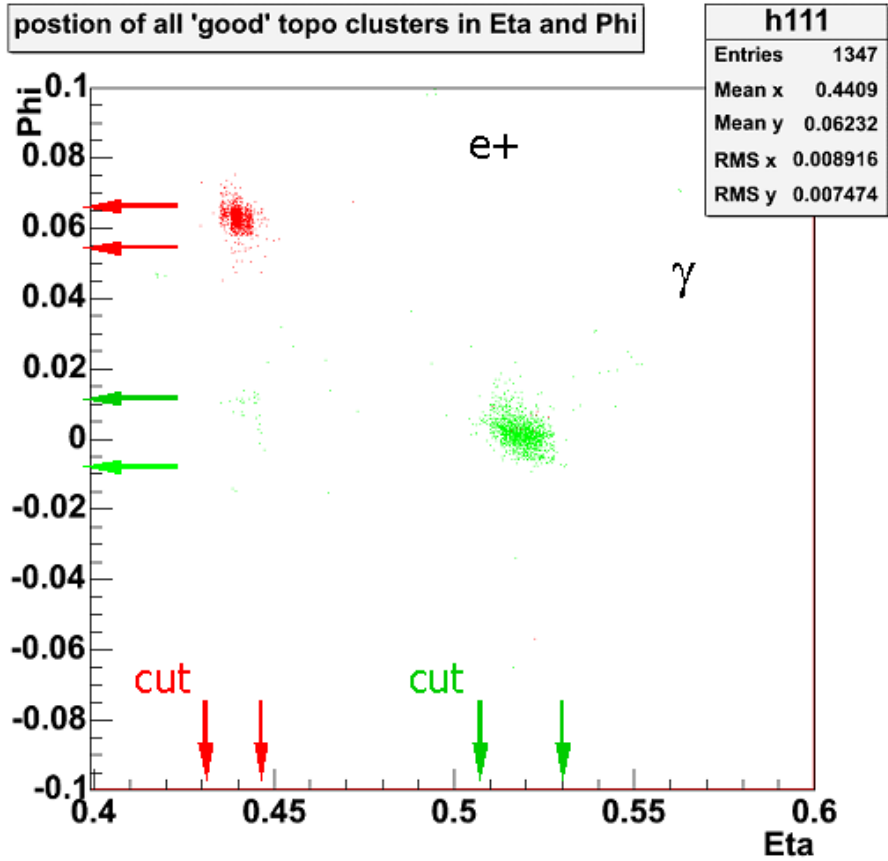


Figure 3: Illustration of the geometrical cut procedure at the example of run #'89. The positions of barycenters of the electron clusters are shown in red, the ones of the photons in green.

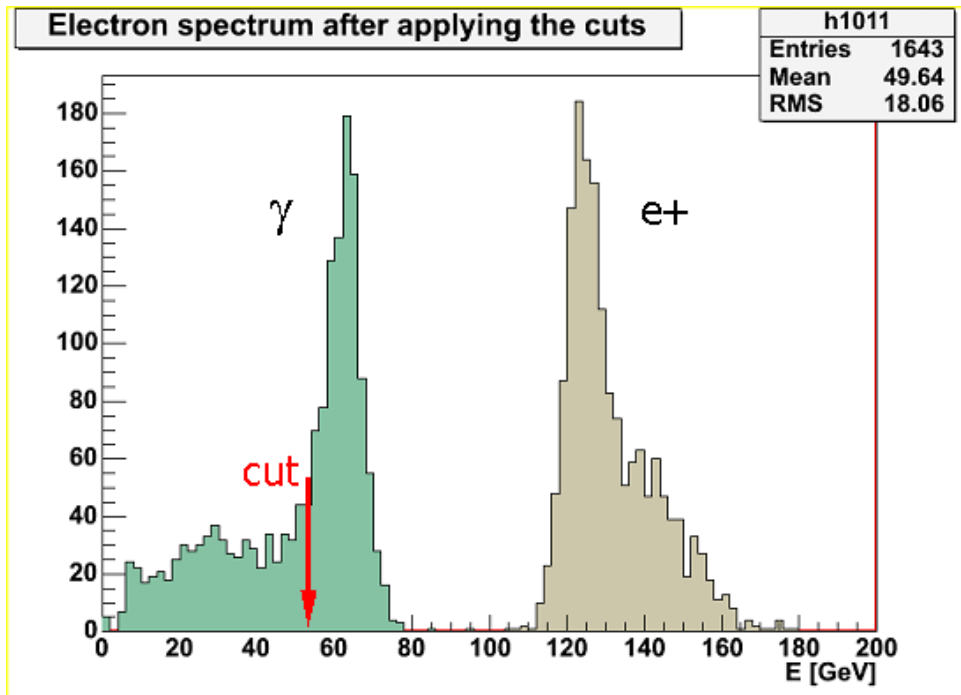


Figure 4: Electron and photon spectra after the application of the geometrical cut for run #'89. Another cut is applied on photon energy: $E_{\gamma} > 55 \text{ GeV}$ (red arrow)

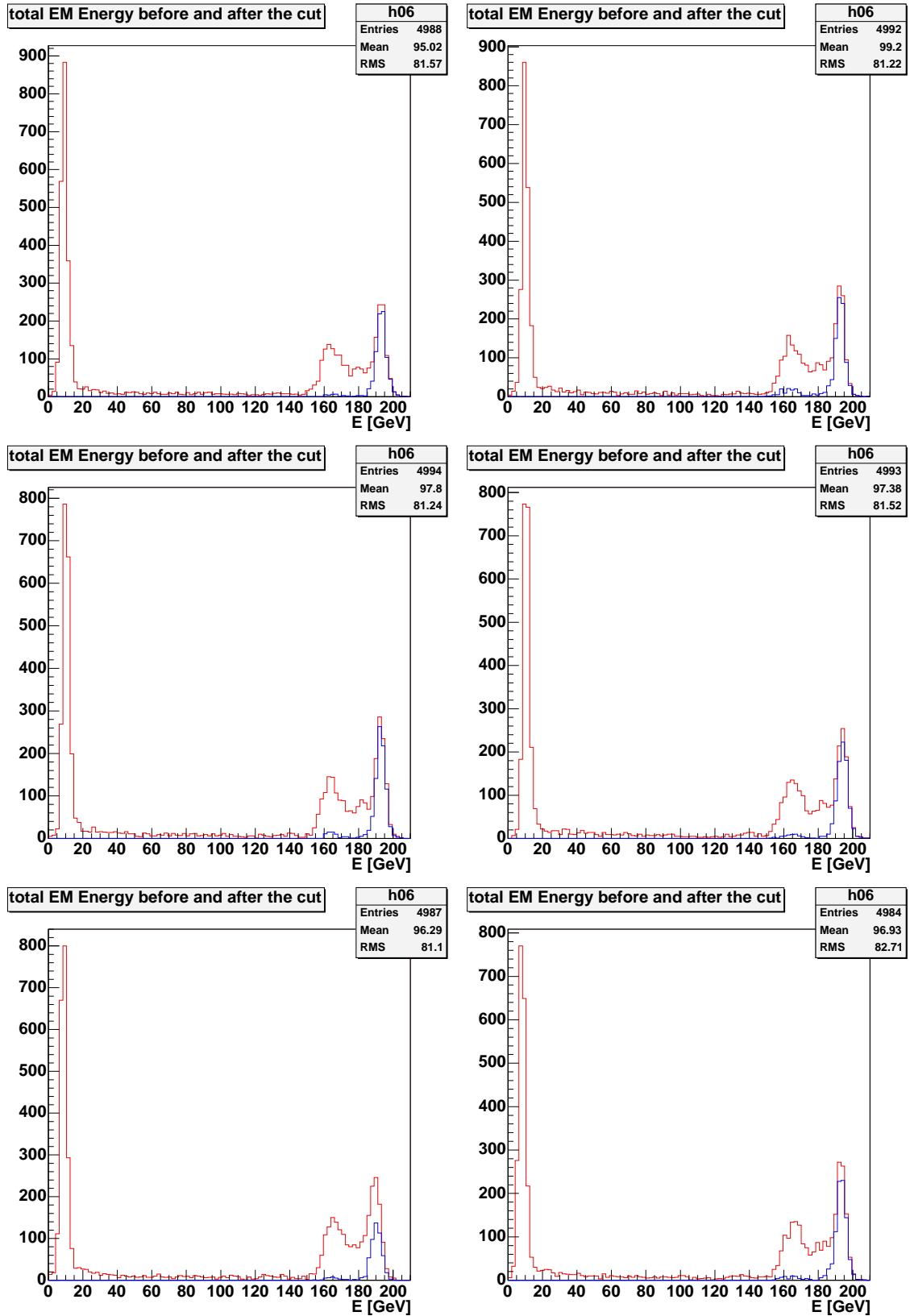


Figure 5: Total energy spectrum before (red) and after (blue) the cut for for all available runs (the runs with a * will not be considered in the further analysis):

top left:	#'66 (comparison run)	top right:	#'83* (-20.9 cm)
middle left:	#'84 (-20.9 cm)	middle right:	#'85 (+20.9 cm)
bottom left:	#'86* (+62.7 cm)	bottom right:	#'89 (+41.8 cm)

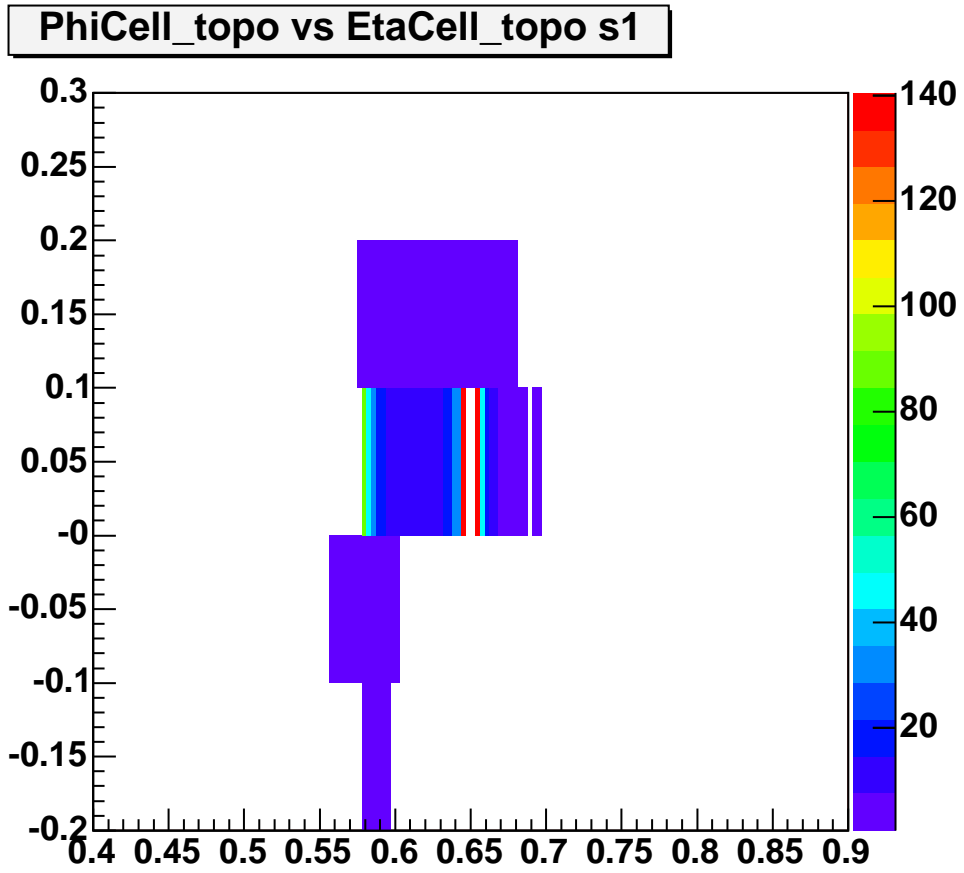


Figure 6: The photon beam hits exactly two dead cells in run #2120986 (+62.7 cm). It will not be considered in the further analysis for this reason

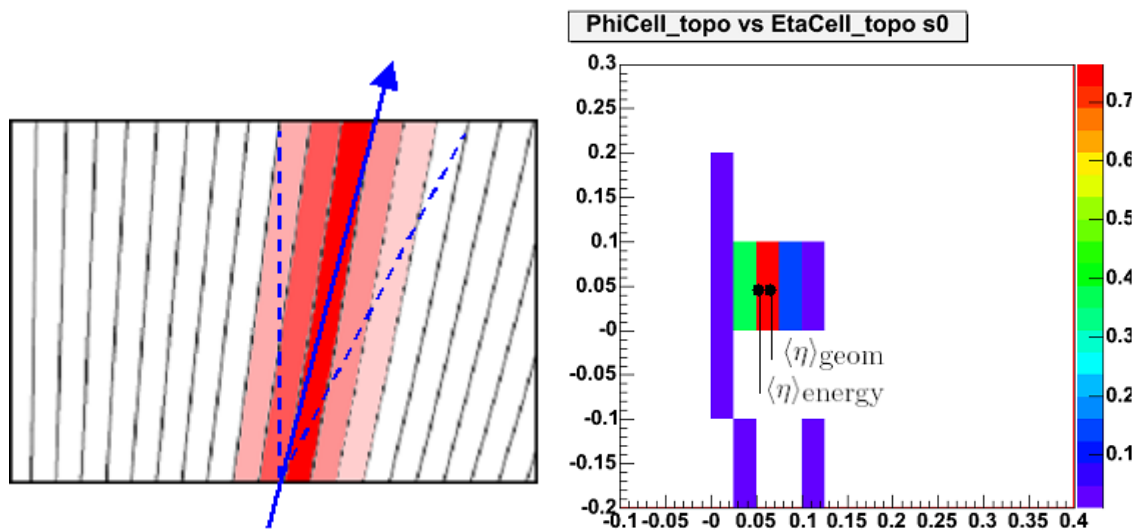


Figure 7: Illustration of the single sampling method.

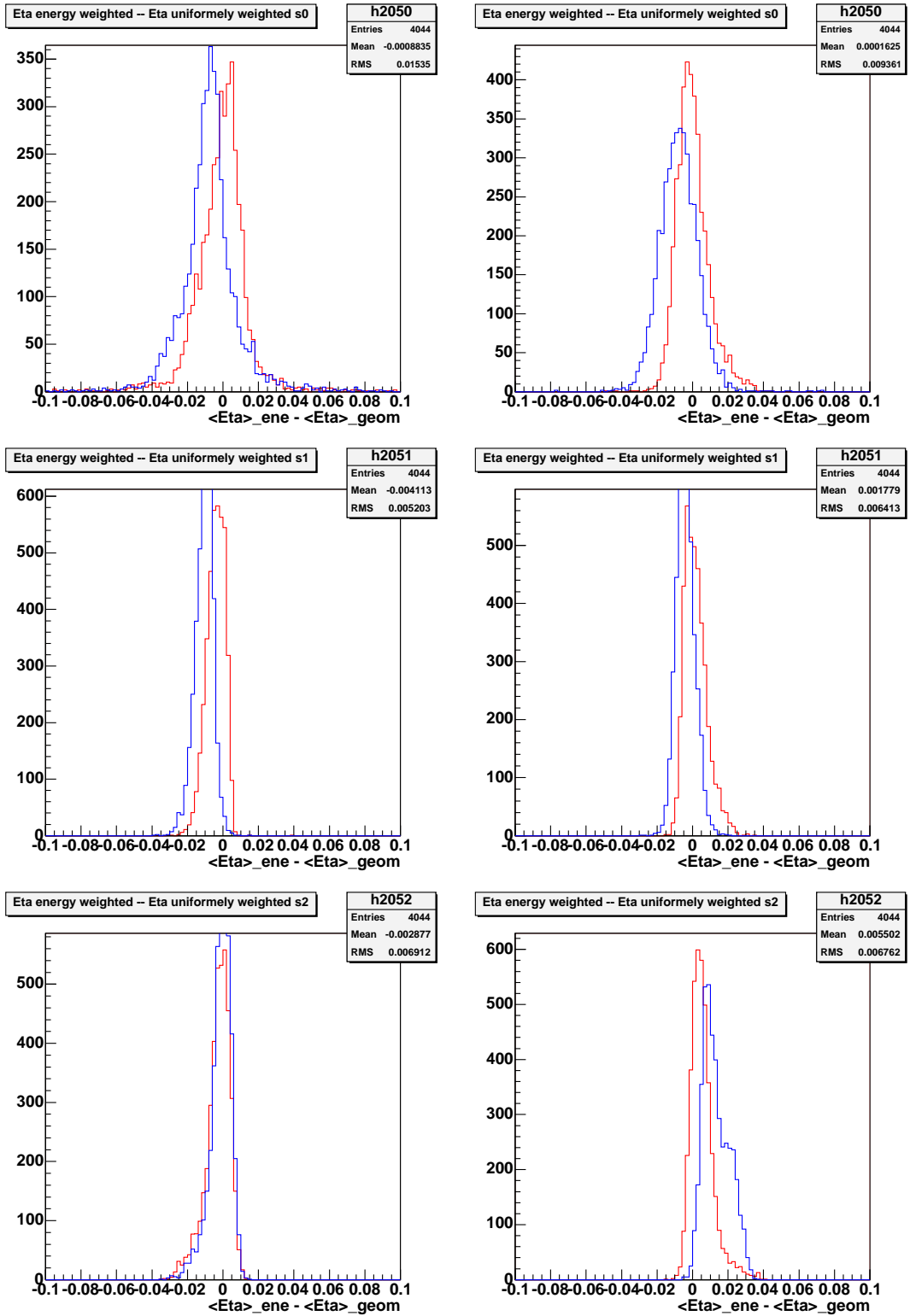


Figure 8: Results of the single sampling method for run #2120984 (-20.9 cm) (blue) compared with a projective run #2120966 (red).

top left: photons, s0 (presampler) **top right:** electrons, s0 (presampler)
middle left: photons, s1 (strips) **middle right:** electrons, s1 (strips)
bottom left: photons, s2 (middle) **bottom right:** electrons, s2 (middle)

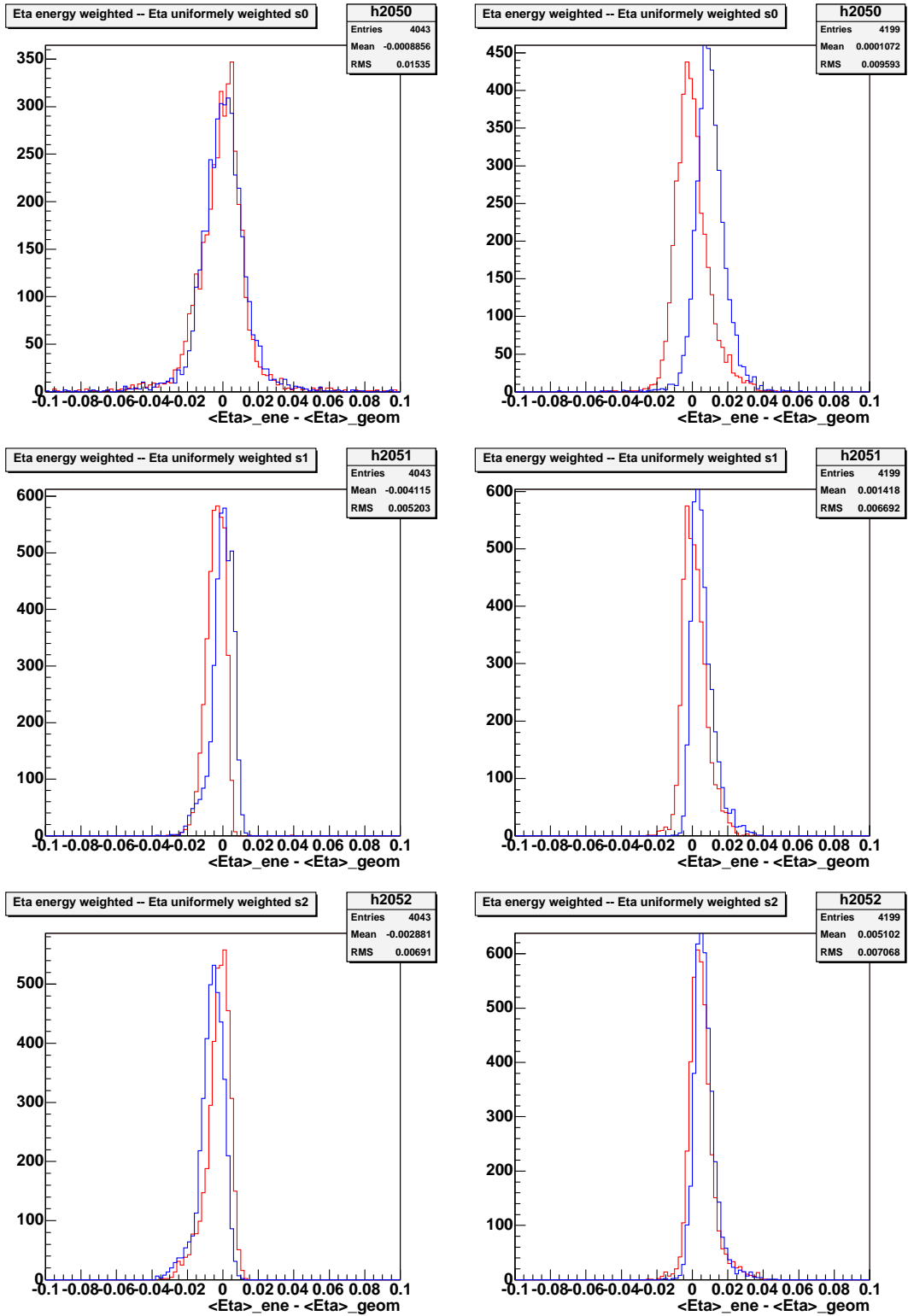


Figure 9: Results of the single sampling method for run #2120985 (+20.9 cm) (blue) compared with a projective run #2120966 (red).

top left: photons, s0 (presampler) **top right:** electrons, s0 (presampler)
middle left: photons, s1 (strips) **middle right:** electrons, s1 (strips)
bottom left: photons, s2 (middle) **bottom right:** electrons, s2 (middle)

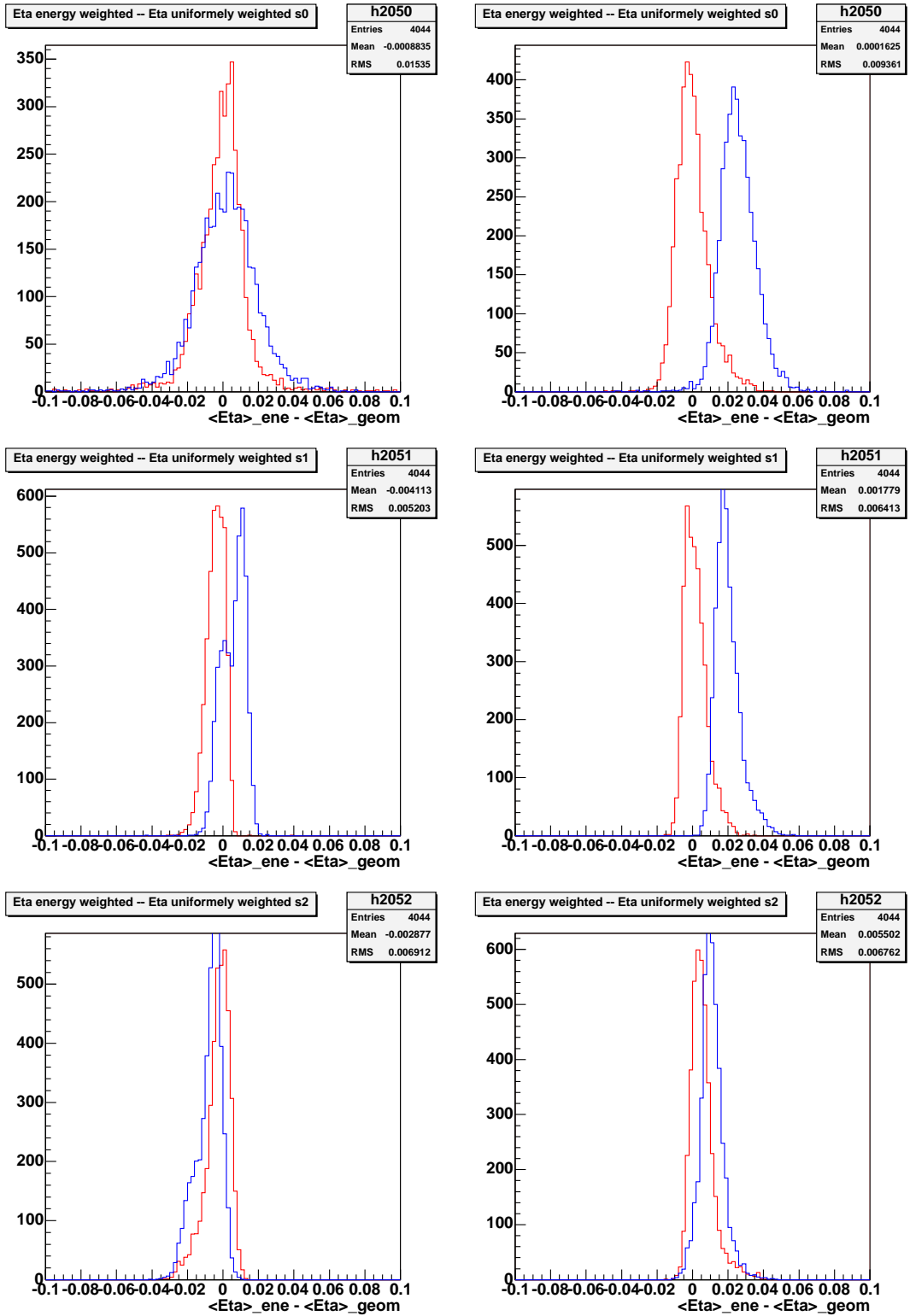


Figure 10: Results of the single sampling method for run #2120989 (+41.8 cm) (blue) compared with a projective run #2120966 (red).

top left: photons, s0 (presampler) **top right:** electrons, s0 (presampler)
middle left: photons, s1 (strips) **middle right:** electrons, s1 (strips)
bottom left: photons, s2 (middle) **bottom right:** electrons, s2 (middle)

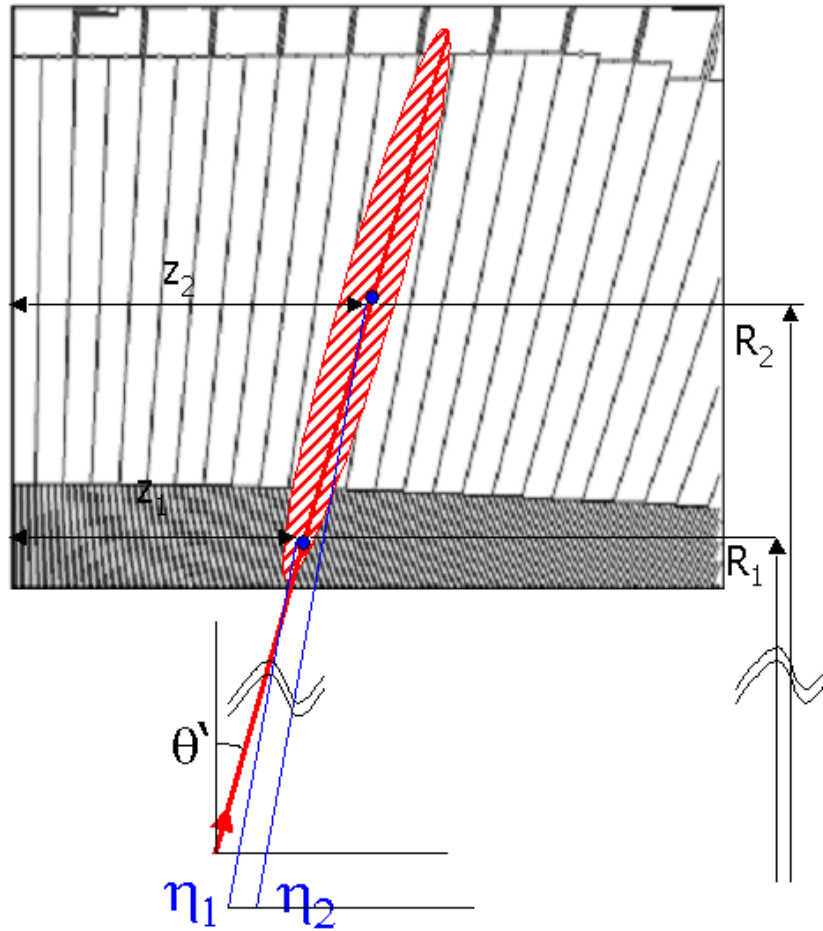


Figure 11: Illustration of the two sampling method.

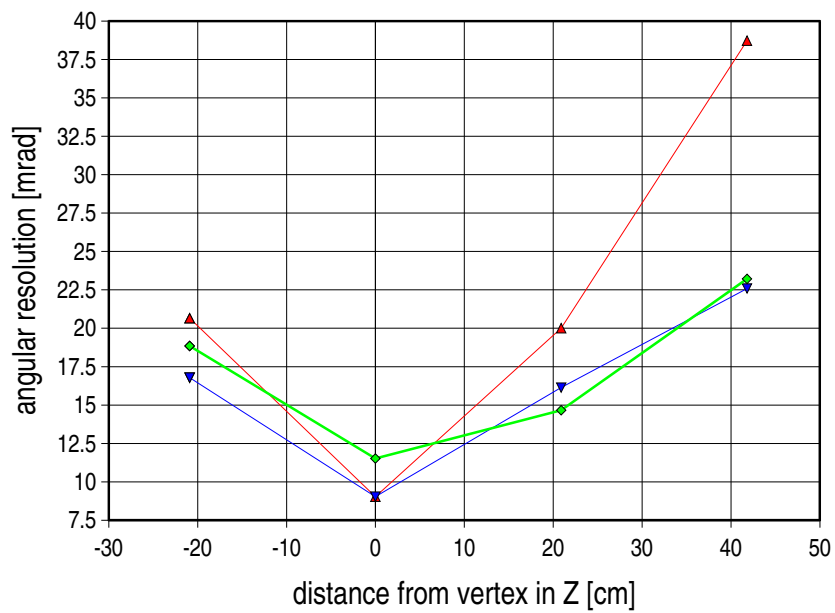


Figure 12: Angular resolution for photons for the ATLAS detector: as found in [4] without corrections (red), with corrections (blue), and as determined in this report with 2004 Combined Test Beam data (green).

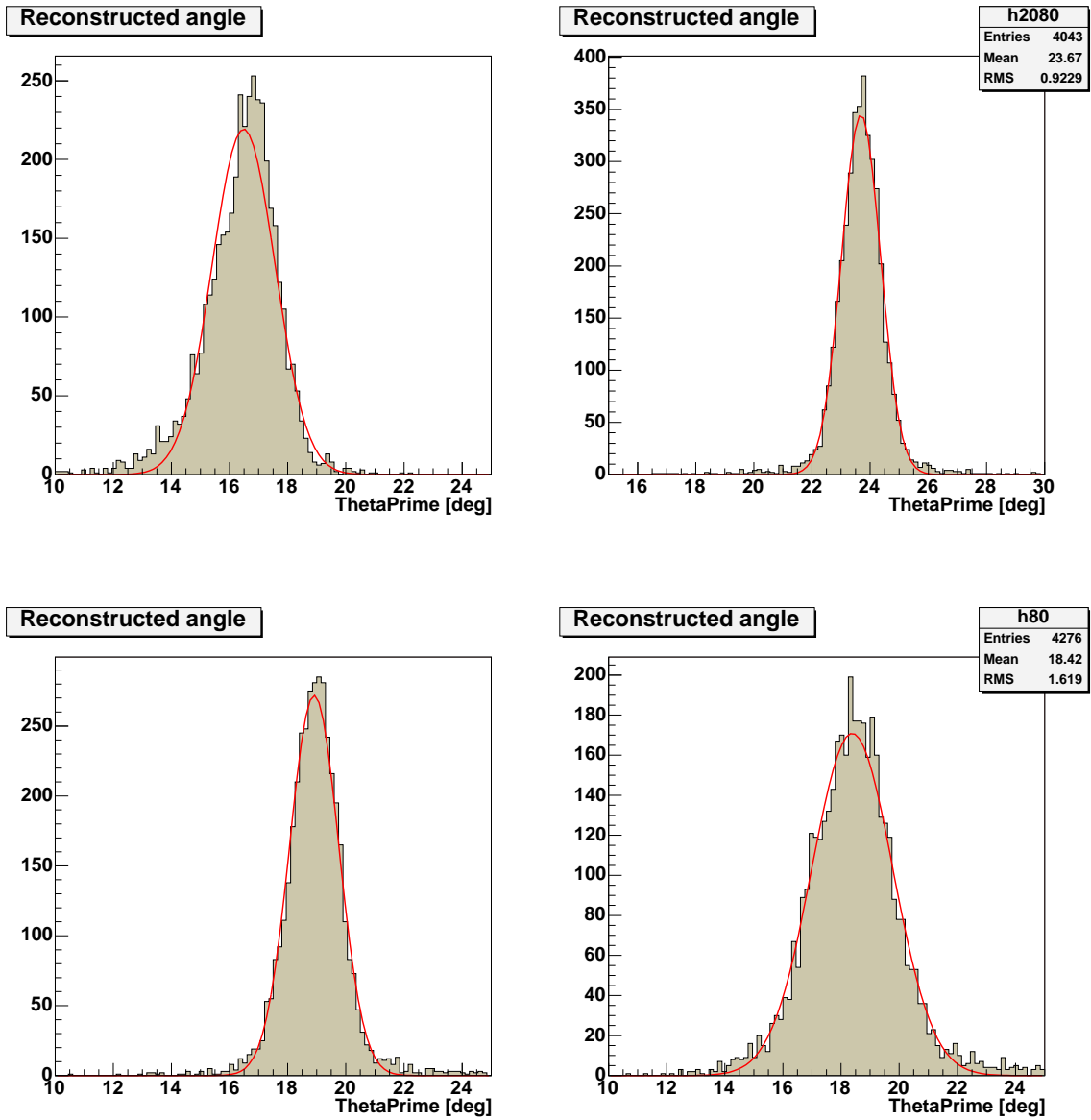


Figure 13: Angular resolution plots for photons for the ATLAS detector as determined with 2004 Combined Test Beam data for different non-projectivities.